IEEE Access
Multidisciplinary ⋮ Rapid Review ⋮ Open Access Journal

Received 19 March 2025, accepted 4 May 2025, date of publication 7 May 2025, date of current version 16 May 2025.

Digital Object Identifier 10.1109/ACCESS.2025.3567637

RESEARCH ARTICLE

Human Presence Detection Sensor Using Polarization Insensitive Metamaterial Absorbers

FARZAD TOFIGH, (Member, IEEE), AND JUSTIN LIPMAN, (Senior Member, IEEE)
School of Electrical and Data Engineering, University of Technology Sydney, Sydney, NSW 2007, Australia

Corresponding author: Farzad Tofigh (farzad.tofigh@uts.edu.au)

This research was conducted by the University of Technology Sydney for National Intelligence Postdoctoral Grant (project number NIPG202309) and funded by the Australian Government.

ABSTRACT Non-invasive crowd estimation has remained a challenging issue among researchers. Methods such as image analysis and Wi-Fi/Bluetooth probing can always be used to identify and track people. Lately, the authors have introduce a non-invasive method for crowd estimation based on ambient RF energy measurements. In this paper, a sensitive sensor based on metamaterials is introduced to measure the variations within an environment of the available RF energy levels for crowd estimation purposes. Considering human body resonance at 2 GHz, a metamaterial absorber is designed to operate at 2.4 GHz while remaining insensitive to polarisation and incident angle. This absorber, is equipped with a feed network and rectifier to efficiently absorb and transfer the maximum available Wi-Fi energy into a measurable DC voltage. To evaluate the performance of the sensor, the proposed structure is fabricated as an array, and its performance is tested in both the lab and a controlled real-world environment.

INDEX TERMS Crowd estimation, metamaterial absorber, electromagnetic energy, EM energy.

I. INTRODUCTION

The rapid expansion of urban environments requires a comprehensive understanding of city infrastructure, environmental dynamics, and the dynamics of resident movement and behavior. Effective urban management depends on optimising public safety, transportation systems, and maximising the efficient use of public spaces. One critical component of these anlysis is the monitoring of crowd density and its distribution which can directly impacts emergency response, resource management, and overall urban livability.

Image processing techniques have been extensively used for crowd monitoring due to their precision in detecting and analysing human activity [1], [2], [3]. However, these methods are inherently constrained by several limitations, including high computational costs, the requirement for extensive camera networks, and significant privacy concerns. The strategic deployment of cameras, along with the continuous processing of high-resolution video feeds, demands considerable resources, making these systems difficult to scale in rapidly expanding urban landscapes.

To overcome these challenges, researchers have explored alternative sensing solutions that leverage the widespread adoption of wireless communication technologies. Approaches such as Wi-Fi and Bluetooth node scanning [4], [5], [6], [7], [8], [9], Bluetooth Low Energy (BLE) [10], and RFID-based detection systems [11] have been explored as viable solutions. These methods rely on the ability to detect wireless signals emitted by mobile devices or RFID tags, enabling the estimation of crowd size and movement patterns. However, their effectiveness depends on individuals carrying devices, which can also introduce privacy concerns as one can be tracked through the device's unique layer 2 network identifier.

A significant breakthrough in crowd density estimation has emerged with the development of passive sensing techniques that utilize commercial off-the-shelf (COTS) Wi-Fi infrastructure. Unlike device-dependent methods, these approaches do not require individuals to carry any specific hardware. Instead, they analyze Wi-Fi Channel State Information (CSI), which captures how wireless signals interact

The associate editor coordinating the review of this manuscript and approving it for publication was Mauro Fadda.

with the surrounding environment, including human presence and motion [12], [13], [14], [15], [16]. CSI-based methods leverage the modulation of Wi-Fi signals as they propagate through space, interacting with obstacles such as walls, furniture, and, most critically, human bodies. By examining variations in signal attenuation, reflection, and scattering, researchers can infer occupancy levels [17], [18], [19], movement trajectories [20], [21], [22], and even specific human activities within a monitored area [15], [23]. However, CSI is highly environment dependent and sensitive to a wide range of ambient factors, including changes in layout, humidity, temperature fluctuations, and even subtle movements of objects, which can significantly distort the signal profile [24], [25]. These variations can degrade model accuracy and stability, particularly if the system was trained under different environmental conditions. In some cases, adversarial manipulation of the environment, whether intentional or incidental, can mislead CSI-based inference systems [26]. To address this, researchers have developed mitigation strategies such as signal filtering, domain adaptation, and robust feature extraction to improve generalization and reliability [13], [15], [27], [28]. Despite these challenges, CSI-based sensing offers a privacy-preserving and infrastructure-compatible alternative to camera-based monitoring, but its success hinges on effective management of environmental variability.

Building upon the omnipresence of Wi-Fi signals, an innovative approach has emerged that utilizes the measurement of electromagnetic (EM) energy to assess crowd density [29]. This technique operates on the principle that human bodies interact with EM waves by absorbing, scattering, and reflecting them. By measuring the energy variations within specific frequency bands, researchers can estimate the number of individuals present in a given area without relying on mobile device signals or intrusive imaging technologies. The accuracy of EM-based crowd sensing is linked to the precision of the measurement systems employed. To enhance sensitivity and efficiency, recent studies have proposed the use of metamaterial perfect absorbers (MPAs) as high-performance EM energy sensors [30]. MPAs possess unique electromagnetic properties that enable them to selectively absorb radiation within targeted frequency bands. Their high efficiency, tunability, and ability to be integrated into various surfaces make them an ideal choice for large-scale, non-intrusive crowd monitoring applications.

The utility of metamaterials extends beyond crowd sensing [31] to include a wide array of applications across multiple scientific and engineering domains. The unique EM properties of MPAs enables advancements in fields such as state detection of insulating oil [32], biosensing for early cancer detection [33], and improvements in energy efficiency, including solar cell performance enhancement [34], thermal emitter optimization [35], and the development of high-performance optical switches [36]. Among these various applications, the sensing capabilities of metamaterials have attracted significant research interest, particularly in enhancing the precision and sensitivity of detection systems across multiple frequency ranges such as refining infrared spectral detection [37], measuring terahertz power [38], and improving the accuracy of digital agriculture and environmental monitoring, including CO_2 concentration analysis [39] and humidity sensing [40]. Additionally, advancements in soil moisture detection [41] and remote water salinity measurement [42] demonstrate the growing versatility of metamaterials in environmental monitoring. Their chemical sensing capabilities have also been leveraged to detect ethanol concentrations through resonance frequency shifts, providing highly sensitive and selective detection methods [43].

Despite these advancements, much of the research on metamaterial-based sensors has predominantly focused on high-frequency applications, particularly in the terahertz regime [44], [45], [46], [47]. While these high-frequency metamaterials have led to breakthroughs in spectroscopy, biomedical imaging, and security screening, the challenge remains in extending their utility to lower-frequency applications with compact and high-efficiency structures.

This study introduces a novel metamaterial-based sensor optimised for human presence detection within the 2.4 GHz Wi-Fi band. Unlike conventional imaging or device-based crowd estimation methods, this sensor leverages passive electromagnetic energy absorption to detect human presence and movement without requiring individuals to carry any specific devices. The proposed metamaterial sensor is designed with a compact periodic structure with dimensions of $19 \times 19 \times 1.2\ mm^3$, designed to achieve perfect absorption (nearly 100%) in the targeted frequency bands. The integration of a single via and an optimized feed network facilitates efficient power transfer to the rectifier, ensuring minimal energy loss while maximising signal acquisition. Such passive sensors provide a sustainable and low-maintenance alternative to active sensor grids, potentially enabling the development of lifetime, battery-less devices that can significantly enhance urban crowd density estimation and monitoring.

The remainder of this paper is organised as follows: Section II offers an overview of the use of EM energy level measurements in crowd detection. Metamaterial sensor designs and simulation results are discussed in Section III. Section IV provides measurement results and V concludes.

II. EM ENERGY LEVELS AND CROWD ESTIMATION

In an environment saturated with electromagnetic (EM) waves, every object introduced into the space alters the distribution and availability of EM energy. The human body, primarily composed of oxygen, carbon, and hydrogen [48], exhibits unique electromagnetic properties, acting as a lossy dielectric material. This means that as EM waves propagate through a space, the human body interacts with them, absorbing and scattering a portion of the energy due to

TABLE 1. Simulation results for different numbers of bodies with various body types [31].

Number of people	Sample type	Average RF energy (dBm)
0	0	0
1	Male	-0.9
1	Female	-0.86
1	Child	-0.6
2	1 Male + 1 Female	-1.7
2	1 Male + 1 Child	-1.5

its dielectric composition. This phenomenon provides an opportunity to utilize EM energy variations for human presence detection; when individuals enter a given area, their bodies absorb ambient EM energy across various frequency bands, altering the local energy distribution.

As discussed in [29] and [31], a series of Finite-Difference Time-Domain (FDTD)-based numerical simulations and experiments are done to provide a clear understanding of EM energy measures and number of people. In this paper we will rely on the measurement results that presented on these publications. For future reference, we represent the data table form [31]. Table 1 shows the results of the energy absorption of human body. The results indicate that the minimum reduction in energy levels is approximately $0.6dB$. It is important to note that absorption levels vary with different body types; for example, bodies with higher fat content tend to show greater absorption rates. Thus, utilising a device that can monitor these variations with greater precision would enhance the accuracy of these estimations.

III. SENSOR DESIGN AND SIMULATION RESULTS

Figure 1 represents the 2D models of the proposed structure for the MPA unit cell with the size of $19 \times 19 \times 1\ mm^3$. The proposed unit cell consists of two layers of *Rogers* 4003 with $\epsilon_r = 3.55$ and loss tangent of 0.0.0027. The metal surface consists of a set of rings, where the radius of $R = 1.55\ mm$ that are connected through symmetric lines with the length of $l_g = 1.1\ mm$ and line width of $W_l = 0.9\ mm$. This layer is connected to the bottom layer using a via with the radius of $R_{via} = 0.25\ mm$ to be connected to the power transmission network. Mid layer that is acting as the ground plane is cut around the via with the width of $W_g = 1mm$. To ensure higher efficiency of the transmission network [49] the thickness of substrate for bottom layer (power transmission layer) is indicated as $h_g = 0.2\ mm$.

Metamaterials are engineered materials composed of periodic metallic structures, typically fabricated on a substrate that modulates the electric permittivity, $\varepsilon(\Omega)$, and magnetic permeability, $\mu(\Omega)$, in relation to the operating frequency. This modulation is a result of the interaction between capacitive and inductive elements within the structure, which are activated by the induced surface currents. At the resonance frequency, the effective impedance of the metamaterial matches that of free space, satisfying the condition $Z(\Omega) = \sqrt{\frac{\mu(\Omega)}{\varepsilon(\Omega)}} = 1$.

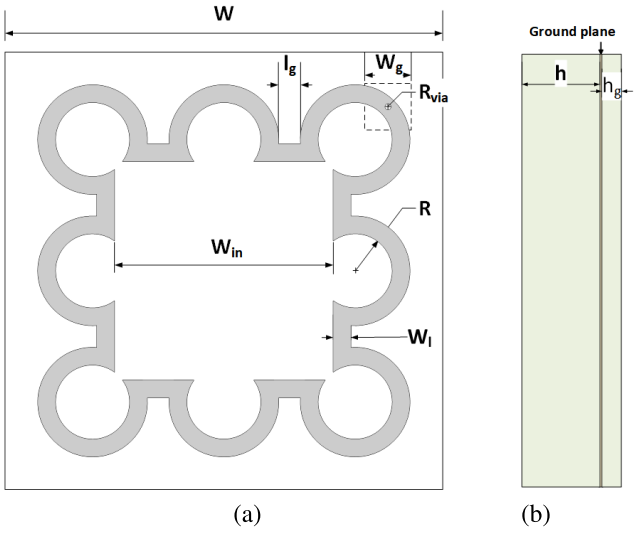

FIGURE 1. Proposed structure of the metamaterial absorber. (a) Top layer. (b) Side view.

The effective impedance can be derived using the reflection and transmission coefficients, as follows:

$$Z(\Omega) = \sqrt{\frac{(1 + S_{11}(\Omega))^2 - S_{21}^2(\Omega)}{(1 - S_{11}(\Omega))^2 - S_{21}^2(\Omega)}},\ \Omega = 2\pi f \qquad (1)$$

And the absorption, $A(\Omega)$, can be calculated according to the definition:

$$A(\Omega) = 1 - \Gamma(\Omega) - T(\Omega) \qquad (2)$$

where $\Gamma(\Omega) = |S_{11}|^2$ and $T(\Omega) = |S_{21}|^2$.

All metamaterial simulations in this work were performed using CST STUDIO SUITE. The frequency domain solver was employed to calculate the absorptivity for different polarisations, incident angles, and S-parameters. A unit cell boundary condition was applied to the structure, enabling adjustments to the polarisation angle (ϕ) and the incident angle (θ). In the second part of the study, the finite integration technique (FIT) and the time domain solver were utilised to modify the input power.

A. EQUIVALENT CIRCUIT

To analyse the effect of each parts of proposed MPA structure on the resonance frequency, Figure 2 (a) illustrates the equivalent circuit based on transmission line theory [50], interpreted as follows:

- Intrinsic impedance of air indicated as Z_0: This part is modeled as unlimited transmission line with constant impedance of 370Ω.
- Top layer resonator that specified as Z_1: This part is modeled as RLC circuit which includes R_1 as an impedance of microstrip structure, L_1 as a inductance of metallic path and C_1 as a created capacitance between metallic patch and metal film.

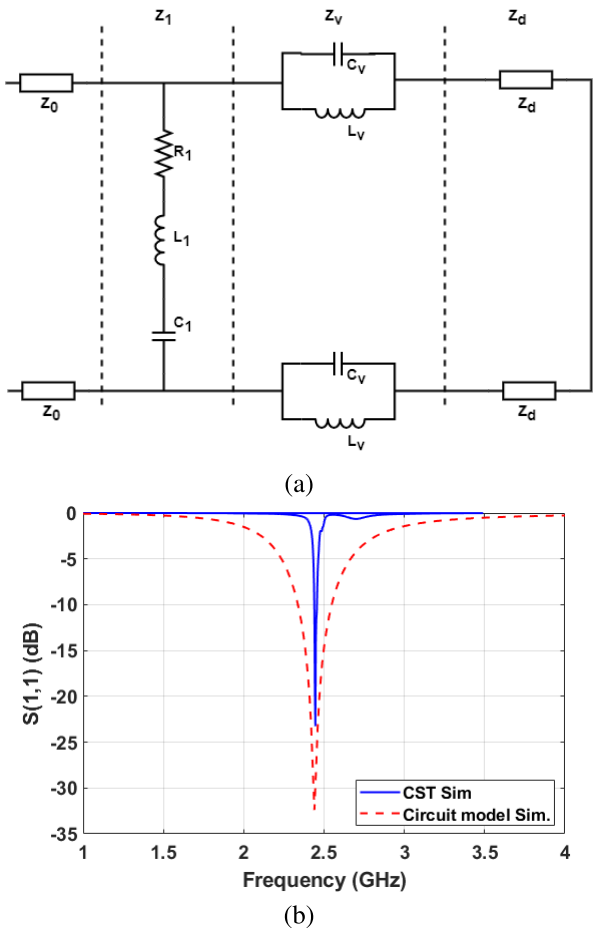

FIGURE 2. (a) Equivalent circuit of the proposed structure, (b) Simulation results of the equivalent circuit model.

- Via impedance is modeled as Z_v: This part is modeled as a LC Circuit due to the created capacitance of via (C_v) and its inductive behaviour (L_v).
- And the substrate is ended with metal film is modeled as Z_d: This part is modeled as a transmission line which $Z_d = 196\Omega$ is the impedance of dielectric and the length of line is $l = 0.75mm$. Moreover the metal film is modeled as shortcut circuit. Z_T can be computed using transmission line theory as below:

$$Z_T(\Omega) = jZ_f tan(\beta l) = j\sqrt{\frac{\mu_r \mu_0}{\varepsilon_r \varepsilon_0}} tan(\frac{2\pi}{\lambda} h) \quad (3)$$

Considering the desired resonance frequency for the structure, the values of each RLC resonators are calculated as: $R_1 = 0.1\Omega$, $L_1 = 1.03\ nH$, $C_1 = 4.13\ pF$, $L_v = 11pH$, $C_v = 0.07\ pF$. Figure 2 (b) presents the simulation results of the equivalent circuit model alongside the results obtained from CST for the structure. This comparison highlights the correlation between the theoretical model and the full-wave simulations, demonstrating the accuracy and consistency of the equivalent circuit approach in representing the structure's behavior.

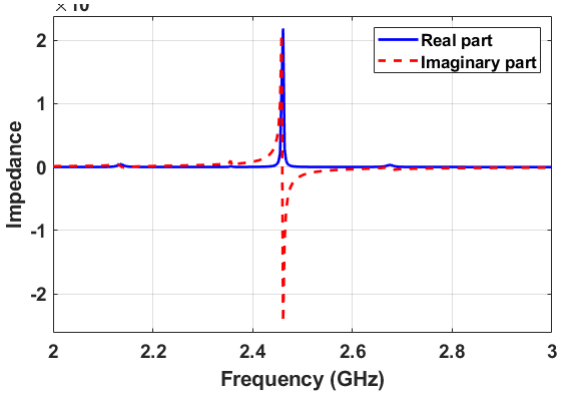

FIGURE 3. Real and imaginary values of Z (Ω).

B. DESIGN PROCEDURE

The interaction between human body absorption and electromagnetic frequencies has been extensively researched, with notable differences in absorption effects across various frequencies [51], [52]. The human body shows two primary resonance frequencies at 60 MHz and 2 GHz [53]. So, measuring the variations of the available electromagnetic energy in the presence of a human being can provide an estimate of the number of people within the area. However, the scarcity of ambient radio frequency (RF) energy at 60 MHz and the corresponding large size of the unit cell at this frequency often necessitates a shift towards more readily available frequencies, such as 2.4 GHz for Wi-Fi, particularly in indoor settings. So, this design aims to provide an accurate sensor to measure variations of Wi-Fi bands at 2.4 GHz by leveraging properties of meta-material perfect absorbers. Furthermore, the proposed symmetric structure offers the capability of absorbing all possible polarisations.

The proposed multi-layer design, offers two separate layers for the absorption and power transmission network. This layered approach decouples the absorption and transmission functions, allowing for independent design optimisation. While the impact of transmission lines in such systems is generally minimal, fine-tuning may be necessary depending on specific performance requirements.

Figure 3, illustrates the real and imaginary components of the effective impedance, demonstrating the metamaterial properties of the structure in targeted frequency.

The structure is polarisation-insensitive, meaning it can absorb EM energy regardless of the polarisation state of incident waves. This characteristic enhances its robustness in real-world conditions where wave orientations vary due to reflections and scattering in indoor environments. Figure 4 shows the E-field, H-field and induced surface current distribution for the absorber at 2.45 GHz. As illustrated in Figure 4(1:a), horizontal rings on the structure are excited when a horizontal linear polarised wave hits the absorber at 2.45 GHz. As the polarisation angle moves from 0 to 90, the

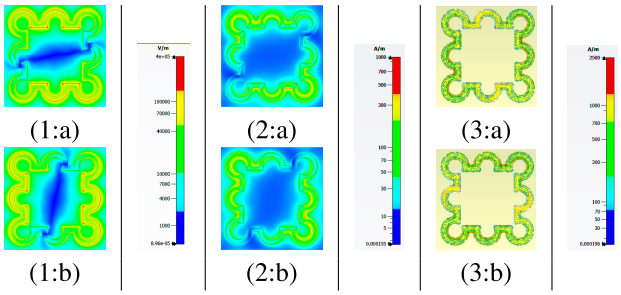

FIGURE 4. (1:*) E-field distribution at (a) 2.45 GHz, TE; (b) 2.45 GHz, TM.(2:*) H-field distribution at (a) 2.45 GHz, TE; (b) 2.45 GHz, TM.(3:*) Induced surface current at (a) 2.45 GHz, TE; (b) 2.45 GHz, TM.

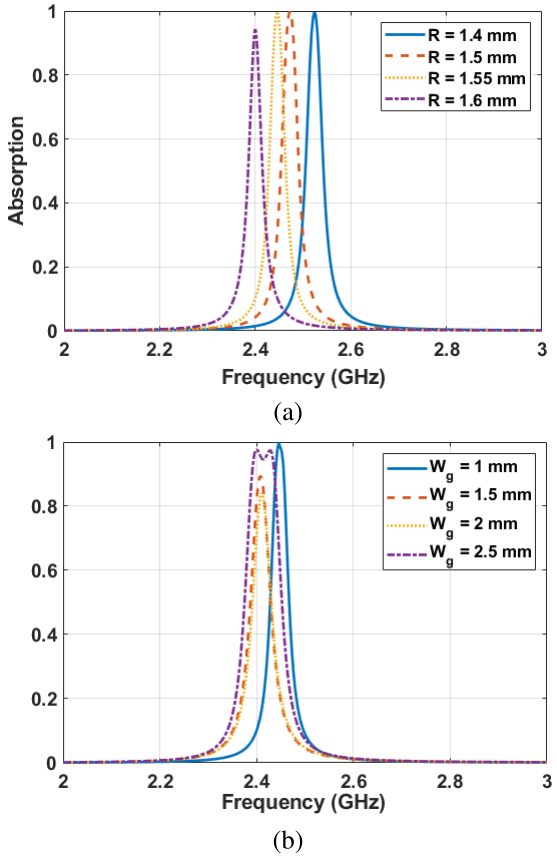

FIGURE 5. Effect of the radius of the rings. (a) Various values of $R = 1.4mm, 1.5mm, 1.55mm, 1.6mm$ with $W_g = 1mm$.(b) Various values of $W_g = 1mm, 1.5mm, 2mm, 2.5mm$ with $R = 1.55\ mm$.

E-field and surface current focus area moves to the vertical set of rings (Figure 4(1:b) and (d)). So, the polarisation insensitivity is guaranteed in the structure.

To investigate effect of parameters on the resonance frequency, Figure 5 (a) illustrates the role of the radius of the ring. As represented by manipulating the radius R of the rings and adjusting the length L_g of the lines, the equivalent electrical length of the resonator changes, and the resonance frequency can be adjusted.

With fixed radius for the rings as $R = 1.55mm$, the effect of the ground plane gap, W_g is investigated. Figure 5 (b) shows

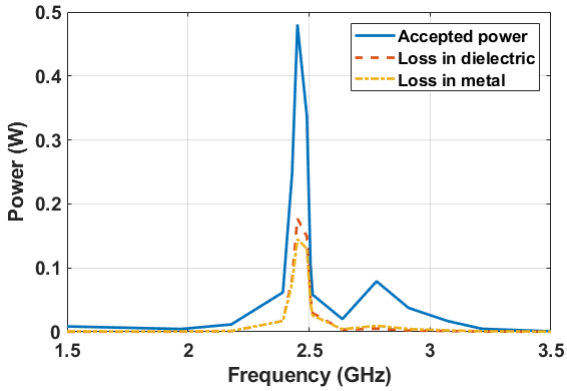

FIGURE 6. Power loss analysis in the structure.

the changes in absorption ratio and resonance frequencies with a small change in gap width. With $W_g = 1\ mm$, the resonance frequency of the structure slightly moves to higher bands as 2.45 GHz. With $W_g = 2.5\ mm$, the resonance frequency can cover broader bandwidth from 2.4 to 2.44 GHz. The gap width of $W_g = 1\ mm$ is fixed in this design.

Absorbers were traditionally designed to trap electromagnetic waves and dissipate them. However, a higher efficiency of the absorbers in catching signals enables new applications in the field of sensing. Similar to most sensing applications, the proposed sensing application in this paper requires the detection of the changes of the available RF energy levels. To provide this function, the loss of the system should be minimal, and the absorbed power should be transmitted and translated to a measurable parameter. Thus, a substrate of *Rogers RO*4003 with the thickness of $h = 1\ mm$ and $h_g = 0.2\ mm$ and loss tangent of 0.0.0027 is selected. Figure 6 illustrates the simulation analysis of power loss within the structure. During the simulations, the structure is positioned in front of a transmitter emitting 0.5 W of power. At the resonance frequency of 2.4 GHz, approximately 92% (0.48 W) of the transmitted power is absorbed by the structure and 0.19 W dissipated as losses in the substrate. Consequently, 0.29 W is effectively transferred to the measurement point.

As mentioned, one of the challenges in using an absorber as a sensor is to transfer the absorbed power and translate it to a measurable parameter. There are various techniques to measure the absorbed power such as using lumped resistors in the top layer and measuring the voltage. However, any added lumped devices on the top layer act as a parasitic element and affect measurements. To avoid this problem, a via is introduced in the structure. The via is used to transfer the induced surface current to the lower layer of the structure where a network of transmission lines and combiners, add up all transferred energy and redirects it to a rectifier so the dc voltage can be easily measured.

According to the application, the structure should be insensitive to the polarisation and incident angle. Figure 7 shows the performance of the proposed structure with various oblique angles and polarisations on TE and TM mode.

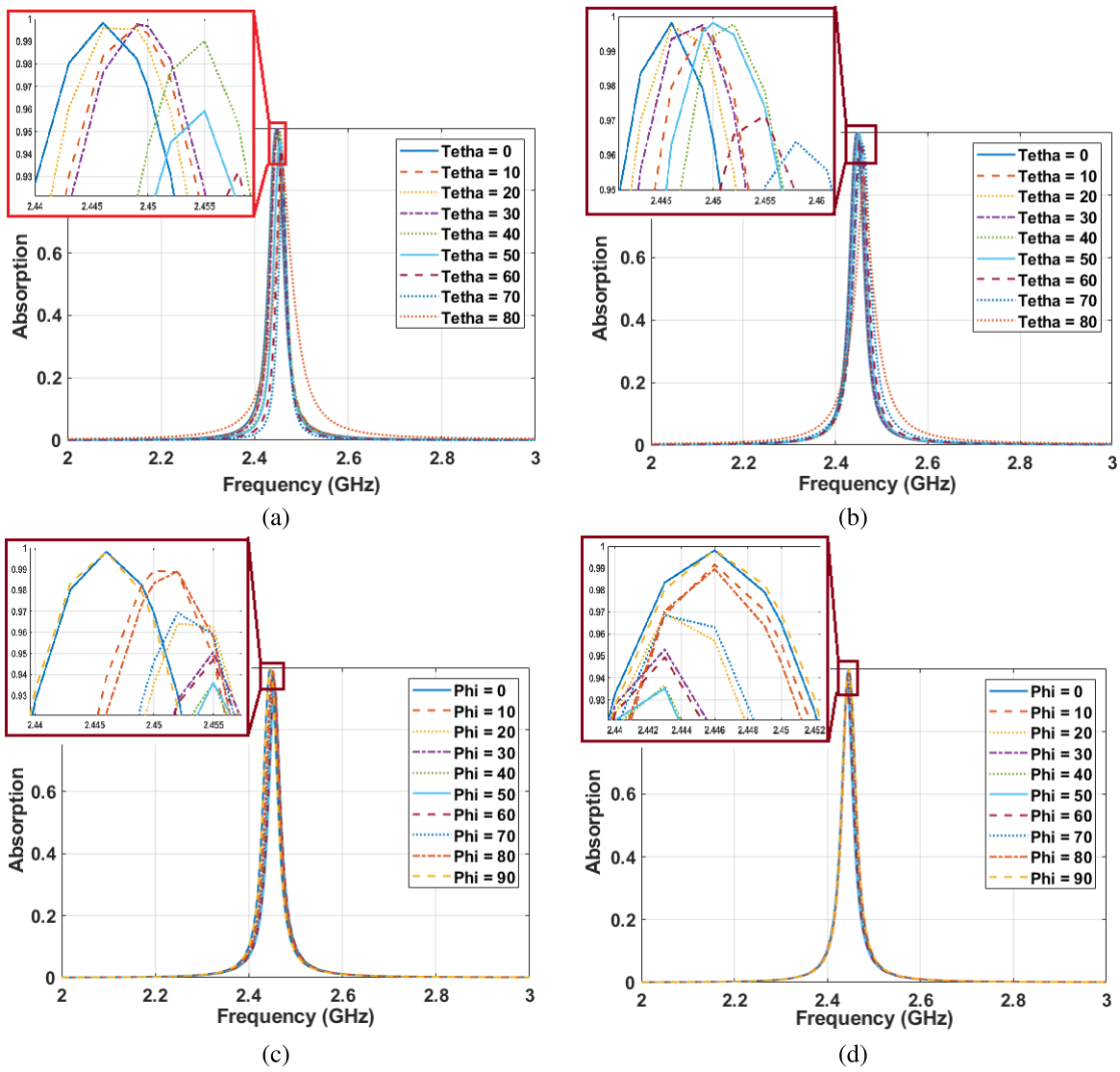

FIGURE 7. Absorption ratio for different angles of the incident wave and polarisation.(a) Absorption ratio for θ in TE mode; (b) Absorption ratio for θ in TM mode; (c) Absorption ratio for ϕ in TE mode; (d) Absorption ratio for ϕ in TM mode.

Despite a small shift at 2.4 GHz, the proposed absorber shows good absorption (over 90%) from *theta* = 0 to *theta* = 70 at both frequencies as shown in Figure 7(a) and (b) for both TE and TM mode. The absorption ratio remains over 95% for all polarisation angles ϕ in TE and TM mode, as shown in Figure 7(c) and (d), respectively.

C. FEED NETWORK

In the design of metasurface arrays, particularly those used for sensing or energy harvesting, the design of feed networks play a critical role in transferring the RF energy to the base measurement point.to the central measurement or rectification point. The performance of the overall system heavily relies on the feed network's ability to minimize power losses, maintain impedance matching, and ensure uniform energy distribution across the array.

To accommodate the feed network within the metasurface architecture, an additional dielectric layer with a thickness of 0.2 mm is incorporated beneath the ground plane. This dedicated layer hosts the microstrip transmission lines that channel the harvested RF energy toward a single rectifier and load, as illustrated in Figure 8. Each resonance cell is connected to the feed network through vertically drilled vias, which facilitate the transfer of RF signals between the metasurface layer and the feed network layer. Since each cell represents a characteristic line impedance of 100Ω, both the vias and the feed network must be designed accurately to ensure impedance matching. The design employs microstrip transmission line theory to determine the optimal line widths corresponding to specific impedance values.

To facilitate impedance transformation within the corporate feed network, a quarter-wavelength ($\lambda_g/4$) transformer

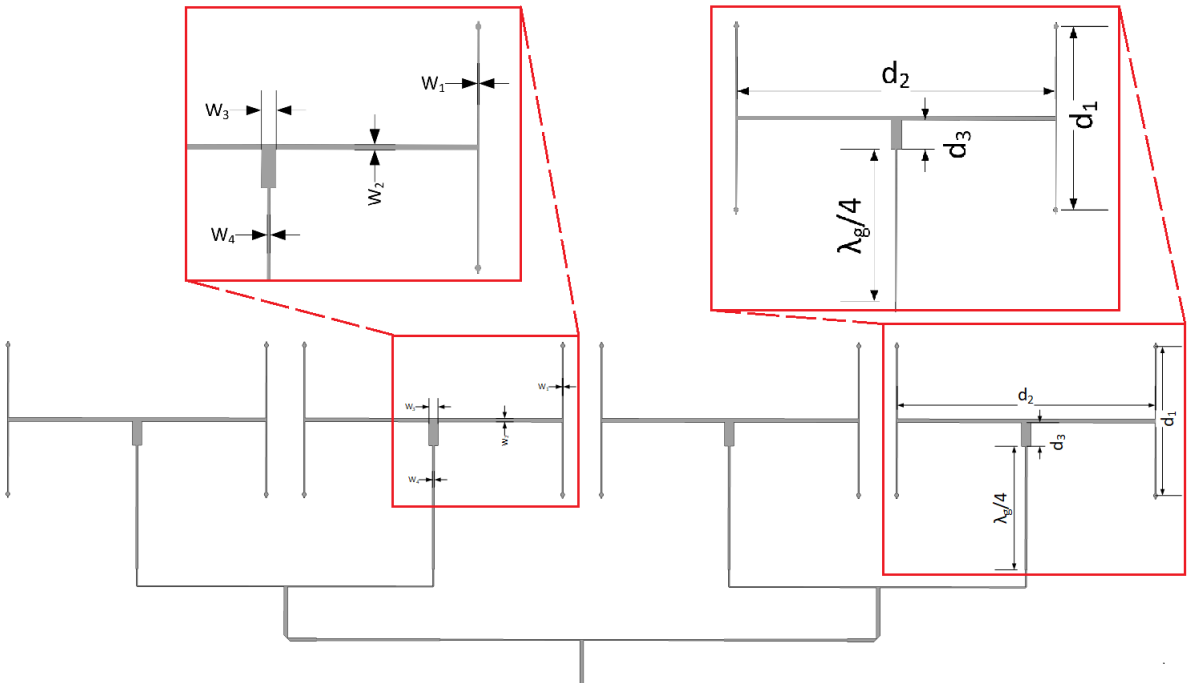

FIGURE 8. The structure of feed network.

TABLE 2. Feed network parameters and values.

Parameter	Value (mm)	Parameter	Value (mm)
d_1	20	W_1	0.12
d_2	34.58	W_2	0.45
d_3	3.18	W_3	1.2
$\lambda_g/4$	16.6	W_4	0.24

is integrated. This transformer is essential for transitioning between different impedance levels while maintaining minimal insertion loss. The width and length of the quarter-wavelength transformer are set to 0.2 mm and 16.6 mm, respectively, based on the guided wavelength λ_g at the operating frequency.

Although energy harvesting systems do not strictly require adherence to a 50Ω impedance standard, a 50Ω load was selected in this design. This choice simplifies the measurement of AC power using conventional power meters with a 50Ω input impedance, ensuring compatibility with standard laboratory equipment. The captured energy from individual resonators is routed through the feed network, aggregated, and delivered to a central measurement point. The key physical parameters of the feed network, including transmission line widths and segment lengths, are summarised in Table 2.

The entire feed network design was simulated using Agilent Advanced Design System (ADS). The results confirmed the network's ability to efficiently combine signals from multiple cells with minimal degradation, ensuring reliable energy transfer to the rectification stage.

TABLE 3. Impedance matching parameters and values.

Parameter	Value (mm)	Parameter	Value (mm)
l_1	7	W_1	3
l_2	2	W_2	3
l_3	5	W_3	13
l_4	5	W_4	0.7
l_5	8	W_5	22
l_6	5	W_6	10
l_s	8	W_s	1

D. IMPEDANCE MATCHING AND RECTIFIER

As discussed, the interaction between the human body and electromagnetic (EM) energy leads to measurable changes in radio frequency (RF) signal energy. By monitoring these variations, it is possible to estimate the number of individuals present in a given area. To facilitate accurate detection, the metasurface sensor must be optimised for efficient signal processing and energy conversion. This requires an impedance matching network that ensures maximum power transfer from the RF feed network to the rectifier, which subsequently converts the captured RF energy into a DC signal suitable for measurement and analysis using an Analog-to-Digital Converters (ADC).

Figure 9 shows the design of the impedance matching circuit, which is critical for ensuring efficient power transfer from the sensor to the rectifier circuit. The circuit is designed to match the standard 50Ω impedance to the input impedance of the rectifier. This minimizes reflection losses, improves RF-to-DC conversion efficiency, and ensures accurate signal measurement.

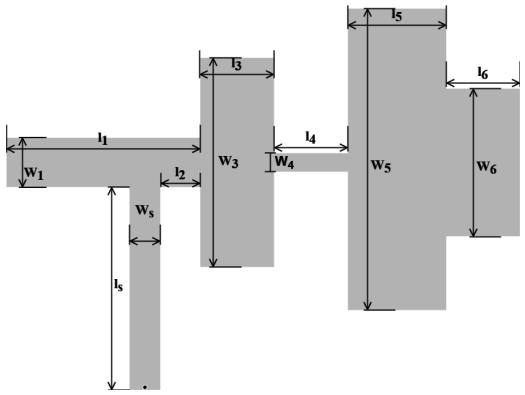

FIGURE 9. Impedance matching circuit.

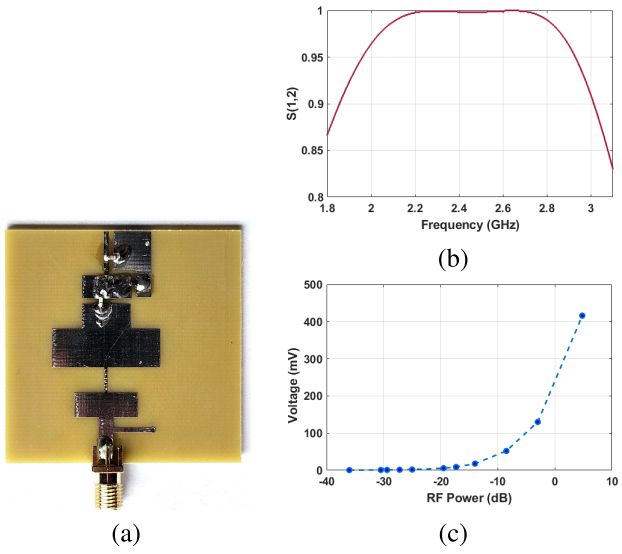

FIGURE 10. (a) Fabricated version of the rectifier circuit, (b) S(1,2) for impedance matching circuit, (c) RF power conversion to DC voltage (mV).

The designed impedance matching circuit utilises microstrip transmission lines, carefully dimensioned to create the desired impedance transformation without relying on lumped components, which can introduce parasitic capacitance and inductance, especially at high frequencies. The design parameters, including the lengths (l_i) and widths (W_i) of the transmission lines and stubs, are optimized based on microstrip transmission line theory. The critical dimensions are summarized in Table 3. The matching network includes a short-circuited stub and series transmission lines to accurately replicate the required resonator characteristics. This network is connected to a rectifier, which consists of a 33 pF capacitor in series with the cathode of a BAT 63-02V Schottky diode, enabling efficient conversion of the RF energy into a measurable DC signal.

The fabricated rectifier circuit and the corresponding measurement results are shown in Figures 10(a) and 10(b) and (c), respectively. The measured S_{11} parameter (Figure 10(b)) of the impedance matching network, demonstrating efficient signal transmission with minimal losses across the desired frequency range. The RF-to-DC conversion efficiency in Figure 10(c), illustrates the relationship between input RF power and the corresponding DC output voltage (in mV). The results confirm that the rectifier achieves high conversion efficiency, validating the effectiveness of both the matching network and the rectifier design.

IV. MPA AS A SENSOR

Metamaterial Perfect Absorbers (MPA) are capable of achieving 100% efficiency at their resonance frequencies, which makes them highly sensitive to small variations in the surrounding electromagnetic environment. This unique capability allows them to detect subtle changes in RF energy levels, making them an excellent choice for replacing traditional antennas in energy measurement applications. Furthermore, metamaterial absorbers are cost-effective and can be easily deployed on a large scale, which enhances their practicality for real-world sensing applications, such as crowd estimation.

The proposed approach is fabricated as an array to evaluate its performance in a real-world environment. Figures 11(a) shows the top layer of the fabricated 2 × 8 array of the proposed structure on a substrate of *Rogers* 4003. The structure is used to test its performance in comparison with the simulation results. Then, the absorber is used to measure the changes of the available RF energy levels in the lab and real environment to validate its proposed application.

To test the fabricated absorber, the structure is fixed in front of the EMC pyramid absorbers to avoid the reflection when the power is radiating. Two AINFOMW quad-ridged horn reference antennas are connected to a ROHDE & SCHWARZ ZNL6 vector network analyser (VNA) to measure parameters S_{11} and S_{12}. Figure 11(a) and (b) represent the measurement setup of the proposed structure and measured S_{11} in comparison with simulation results, respectively. The measurements demonstrate strong alignment with the simulation results, exhibiting perfect absorption at the target resonance frequency of 2.45 GHz, despite a minor shift in resonance frequencies. Additionally, the proposed structure has been tested to assess its performance under varying oblique angles and polarisation conditions. The absorber maintains high absorption efficiency, with strong performance observed from $\theta = 0$ to $\theta = 70$ and absorption consistently above 90% across all polarisation angles (ϕ).

Upon confirmation of the performance of the absorber, the whole structure as a sensor is tested. Figure 12(a) represents the measurement setup to test the performance of the structure in the anechoic chamber with different input powers. The sensor sits within 1.5 meters from the transmission power. Figure 12(b) shows the measurement results for measurable values for the voltage with respect to various levels of transmitted power. Setting transmitting power as 0 *dBm*, the measured voltage is 0.28 (mV) at 2.4 GHz.

The proposed metamaterial absorber in this study is designed to function as a sensor by measuring fluctuations in RF energy and converting these changes into DC voltage,

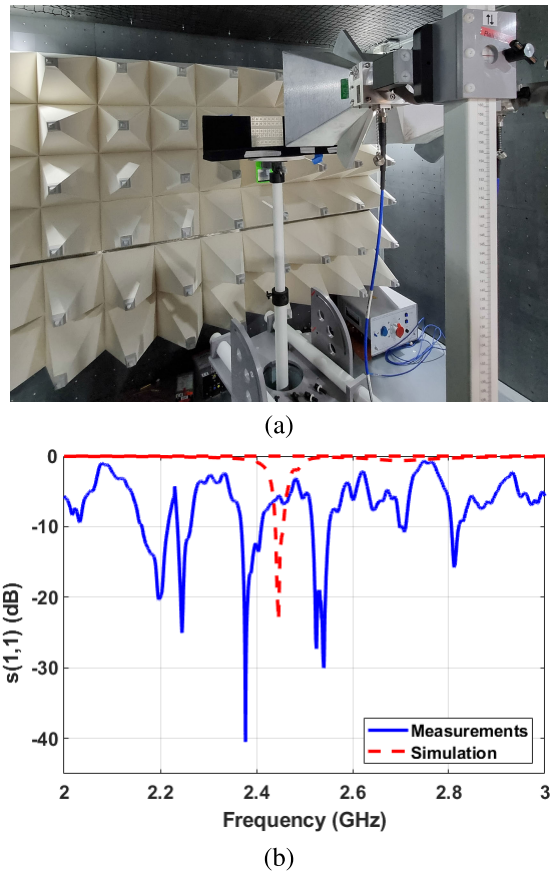

FIGURE 11. (a) Absorption measurement setup, (b) S(1,1) measurements.

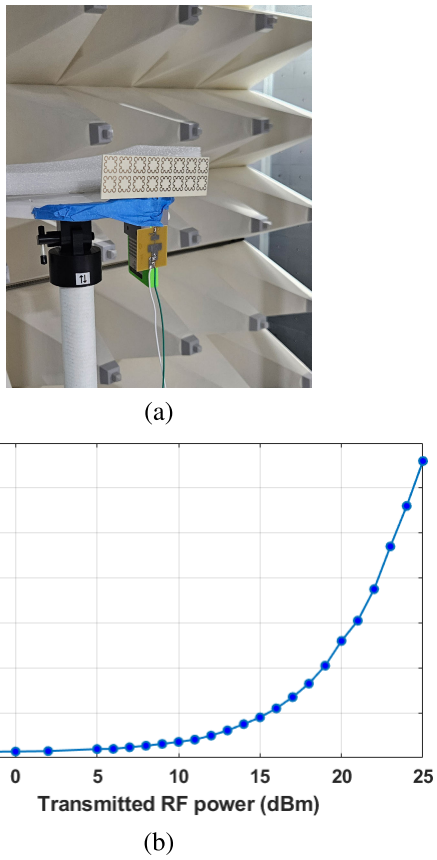

FIGURE 12. (a) Test setup for RF to DC conversion measurements. (b) Measure of voltage for various transmitted RF power.

which can be easily measured. The sensitivity of the absorber, as a crowd estimation sensor, is defined by the amount of output voltage it generates in response to variations in the surrounding RF energy levels.

A. CROWN ESTIMATION IN CONTROLLED ENVIRONMENT

To evaluate the performance of the proposed system in real-world scenarios, a series of sensing units were installed within a controlled room environment. The objective was to measure DC voltage variations corresponding to the presence of varying numbers of people. Given the anticipated low magnitude of voltage variations, multiple sensing units were connected in series to enhance measurement sensitivity. The room setup is illustrated in Figure 13. For these experiments, seven sensing units were configured in series, and the baseline DC voltage was recorded under initial, undisturbed conditions. The sensors were aligned along a single wall, spaced at intervals of 50 cm. Notably, the room featured a glass door and a section of glass wall, whose potential influence on results is addressed later in the discussion. Each test was repeated ten times to ensure reliability and repeatability.

The presence of a human in the room caused a detectable voltage drop. Although the measured voltages exhibited slight fluctuations, the average of ten samples (collected over 10 seconds) was calculated to obtain a consistent value. It is important to note that the RF energy levels within the room could vary slightly, which might influence the measured

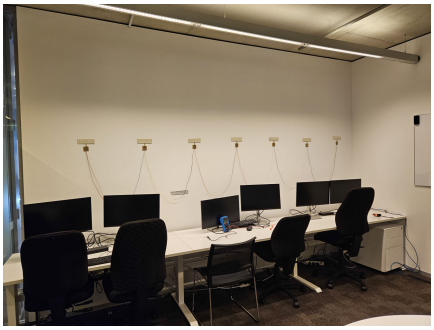

FIGURE 13. Test environment.

TABLE 4. Normalised voltage measurements for different number of people.

Number of People	Rescaled Voltage
Empty room (0)	100
1	89
2	79
3	69
4	60
6	54

voltage values. On average, each individual caused a voltage drop of approximately 3 mV in the system. Table 4 presents the normalized voltage drops corresponding to different numbers of people in the room, with an empty room serving as the baseline (normalised to 100).

Interestingly, the voltage drop became detectable even before a person fully entered the room. As a person approached the glass door, the system recorded 0.5 mV drop in the measured voltage. This level of sensitivity highlights the system's ability to detect human presence before physical entry into the room.

V. CONCLUSION

A metamaterial-based human presence detection and crowd estimation senor has been presented in this paper. The proposed solution consists of a metamaterial absorber along with a rectifier that offers a method to measure the variations of RF energy in any environment. The proposed metamaterial structure was fabricated as an array of 2 × 8 elements and tested in an anechoic chamber. A number of sensing units were manufactured and the combined performance was tested in controlled real-world environment. Experimental validation in controlled environments demonstrated that the sensor consistently detected human presence, with measurable voltage variations corresponding to different crowd densities. Notably, the sensor was sensitive enough to register human presence even before individuals fully entered the monitored area. The proposed sensor design is compact, cost-effective, and easily deployable in urban settings, making it a viable addition to smart city infrastructure for applications such as crowd monitoring, public safety optimization, and resource management.

REFERENCES

[1] S. A. M. Saleh, S. A. Suandi, and H. Ibrahim, "Recent survey on crowd density estimation and counting for visual surveillance," *Eng. Appl. Artif. Intell.*, vol. 41, pp. 103–114, May 2015.

[2] V. A. Sindagi and V. M. Patel, "A survey of recent advances in CNN-based single image crowd counting and density estimation," *Pattern Recognit. Lett.*, vol. 107, pp. 3–16, May 2018.

[3] J. M. Grant and P. J. Flynn, "Crowd scene understanding from video: A survey," *ACM Trans. Multimedia Comput., Commun., Appl.*, vol. 13, no. 2, p. 19, 2017.

[4] M. Handte, M. U. Iqbal, S. Wagner, W. Apolinarski, P. J. Marrón, E. M. M. Navarro, S. Martinez, S. I. Barthelemy, and M. G. Fernández, "Crowd density estimation for public transport vehicles," in *Proc. EDBT/ICDT Workshops*, 2014, pp. 315–322.

[5] J. Weppner, B. Bischke, and P. Lukowicz, "Monitoring crowd condition in public spaces by tracking mobile consumer devices with WiFi interface," in *Proc. ACM Int. Joint Conf. Pervasive Ubiquitous Comput., Adjunct*, Heidelberg, Germany, Sep. 2016, pp. 1363–1371.

[6] M. Delafontaine, M. Versichele, T. Neutens, and N. Van de Weghe, "Analysing spatiotemporal sequences in Bluetooth tracking data," *Appl. Geography*, vol. 34, pp. 659–668, May 2012. [Online]. Available: http://www.sciencedirect.com/science/article/pii/S014362281200029X

[7] L. Schauer, M. Werner, and P. Marcus, "Estimating crowd densities and pedestrian flows using wi-fi and Bluetooth," in *Proc. 11th Int. Conf. Mobile Ubiquitous Syst., Comput., Netw. Services*, 2014, pp. 171–177.

[8] A. Stopczynski, J. E. Larsen, S. Lehmann, L. Dynowski, and M. Fuentes, "Participatory Bluetooth sensing: A method for acquiring spatio-temporal data about participant mobility and interactions at large scale events," in *Proc. IEEE Int. Conf. Pervasive Comput. Commun. Workshops (PERCOM Workshops)*, Mar. 2013, pp. 242–247.

[9] F. Tofigh, G. Mao, J. Lipman, and M. Abolhasan, "Crowd density mapping based on Wi-Fi measurements on train platforms," in *Proc. 12th Int. Conf. Signal Process. Commun. Syst. (ICSPCS)*, Dec. 2018, pp. 1–7.

[10] A. Basalamah, "Sensing the crowds using Bluetooth low energy tags," *IEEE Access*, vol. 4, pp. 4225–4233, 2016.

[11] M. Yamin and Y. Ades, "Crowd management with RFID and wireless technologies," in *Proc. 1st Int. Conf. Netw. Commun.*, Dec. 2009, pp. 439–442.

[12] F. Adib and D. Katabi, "See through walls with WiFi!" in *Proc. ACM SIGCOMM Conf. SIGCOMM*, Aug. 2013, pp. 75–86.

[13] Y. He, Y. Chen, Y. Hu, and B. Zeng, "WiFi vision: Sensing, recognition, and detection with commodity MIMO-OFDM WiFi," *IEEE Internet Things J.*, vol. 7, no. 9, pp. 8296–8317, Sep. 2020.

[14] H. Zou, Y. Zhou, J. Yang, H. Jiang, L. Xie, and C. J. Spanos, "DeepSense: Device-free human activity recognition via autoencoder long-term recurrent convolutional network," in *Proc. IEEE Int. Conf. Commun. (ICC)*, May 2018, pp. 1–6.

[15] F. Meneghello, D. Garlisi, N. D. Fabbro, I. Tinnirello, and M. Rossi, "SHARP: Environment and person independent activity recognition with commodity IEEE 802.11 access points," *IEEE Trans. Mobile Comput.*, vol. 22, no. 10, pp. 6160–6175, Oct. 2023.

[16] K. Qian, C. Wu, Z. Yang, Y. Liu, and K. Jamieson, "Widar: Decimeter-level passive tracking via velocity monitoring with commodity Wi-Fi," in *Proc. 18th ACM Int. Symp. Mobile Ad Hoc Netw. Comput.*, Jul. 2017, pp. 1–10.

[17] H. Choi, M. Fujimoto, T. Matsui, S. Misaki, and K. Yasumoto, "Wi-CaL: WiFi sensing and machine learning based device-free crowd counting and localization," *IEEE Access*, vol. 10, pp. 24395–24410, 2022.

[18] L. Zhang, Y. Zhang, B. Wang, X. Zheng, and L. Yang, "WiCrowd: Counting the directional crowd with a single wireless link," *IEEE Internet Things J.*, vol. 8, no. 10, pp. 8644–8656, May 2021.

[19] W. Xi, J. Zhao, X.-Y. Li, K. Zhao, S. Tang, X. Liu, and Z. Jiang, "Electronic frog eye: Counting crowd using WiFi," in *Proc. IEEE Conf. Comput. Commun.*, Apr. 2014, pp. 361–369.

[20] C. Wu, Z. Yang, Z. Zhou, X. Liu, Y. Liu, and J. Cao, "Non-invasive detection of moving and stationary human with WiFi," *IEEE J. Sel. Areas Commun.*, vol. 33, no. 11, pp. 2329–2342, Nov. 2015.

[21] X. Tong, Y. Wan, Q. Li, X. Tian, and X. Wang, "CSI fingerprinting localization with low human efforts," *IEEE/ACM Trans. Netw.*, vol. 29, no. 1, pp. 372–385, Feb. 2021.

[22] H. Yu, B. Yang, J. Liu, and G.-J. Yu, "Passive human trajectory tracking study in indoor environment with CSI," in *Proc. Int. Conf. Netw. Netw. Appl. (NaNA)*, Oct. 2018, pp. 372–377.

[23] Y. Zhang, A. Cheng, B. Chen, Y. Wang, and L. Jia, "A location-independent human activity recognition method based on CSI: System, architecture, implementation," *IEEE Trans. Mobile Comput.*, vol. 23, no. 5, pp. 4793–4805, May 2024.

[24] Z. Shi, Q. Cheng, J. A. Zhang, and R. Yi Da Xu, "Environment-robust WiFi-based human activity recognition using enhanced CSI and deep learning," *IEEE Internet Things J.*, vol. 9, no. 24, pp. 24643–24654, Dec. 2022.

[25] J. Yang, Y. Liu, Z. Liu, Y. Wu, T. Li, and Y. Yang, "A framework for human activity recognition based on WiFi CSI signal enhancement," *Int. J. Antennas Propag.*, vol. 2021, pp. 1–18, Feb. 2021.

[26] A. Sharma, D. Mishra, S. Jha, and A. Seneviratne, "Wi-spoof: Generating adversarial wireless signals to deceive Wi-Fi sensing systems," *J. Inf. Secur. Appl.*, vol. 91, Jun. 2025, Art. no. 104052.

[27] D. Khan and I. W. Ho, "CrossCount: Efficient device-free crowd counting by leveraging transfer learning," *IEEE Internet Things J.*, vol. 10, no. 5, pp. 4049–4058, Mar. 2023.

[28] H. Zou, Y. Zhou, J. Yang, W. Gu, L. Xie, and C. Spanos, "FreeCount: Device-free crowd counting with commodity WiFi," in *Proc. IEEE Global Commun. Conf.*, Dec. 2017, pp. 1–6.

[29] F. Tofigh, M. Amiri, N. Shariati, J. Lipman, and M. Abolhasan, "Crowd estimation using electromagnetic wave power-level measurements: A proof of concept," *IEEE Trans. Veh. Technol.*, vol. 69, no. 1, pp. 784–792, 2020, doi: 10.1109/TVT.2019.2955223.

[30] N. Landy, S. Sajuyigbe, J. J. Mock, D. R. Smith, and W. J. Padilla, "Perfect metamaterial absorber," *Phys. Rev. Lett.*, vol. 100, no. 20, May 2008, Art. no. 207402.

[31] F. Tofigh, M. Amiri, N. Shariati, J. Lipman, and M. Abolhasan, "Polarization-insensitive metamaterial absorber for crowd estimation based on electromagnetic energy measurements," *IEEE Trans. Antennas Propag.*, vol. 68, no. 3, pp. 1458–1467, Mar. 2020.

[32] Y. Zhao, Z. Zhu, K. Zhao, Y. Zhao, and C. Zhang, "An insulating oil refractive index sensor based on multiband High-Q terahertz metamaterials," *IEEE Sensors J.*, vol. 24, no. 21, pp. 34337–34346, Nov. 2024.
[33] M. Y. Azab, M. F. O. Hameed, A. M. Nasr, and S. S. A. Obayya, "Highly sensitive metamaterial biosensor for cancer early detection," *IEEE Sensors J.*, vol. 21, no. 6, pp. 7748–7755, Mar. 2021.
[34] J. Hao, L. Zhou, and M. Qiu, "Nearly total absorption of light and heat generation by plasmonic metamaterials," *Phys. Rev. B, Condens. Matter*, vol. 83, no. 16, Apr. 2011, Art. no. 165107.
[35] M. Diem, T. Koschny, and C. M. Soukoulis, "Wide-angle perfect absorber/thermal emitter in the terahertz regime," *Phys. Rev. B, Condens. Matter*, vol. 79, no. 3, Jan. 2009, Art. no. 033101.
[36] M. Hajizadegan, V. Ahmadi, and M. Sakhdari, "Design and analysis of ultrafast and tunable all optical metamaterial switch enhanced by metal nanocomposite," *J. Lightw. Technol.*, vol. 31, no. 12, pp. 1877–1883, May 6, 2013.
[37] A. Ishikawa, "Infrared metamaterials for high-sensitive surface-enhanced molecular detection," in *Proc. URSI Asia–Pacific Radio Sci. Conf. (URSI AP-RASC)*, Aug. 2016, pp. 1–3.
[38] K. Y. Park, N. Wiwatcharagoses, A. Baczewski, and P. Chahal, "A novel terahertz power meter using metamaterial-inspired thin-film absorber," in *Proc. Int. Conf. Infr., Millim., Terahertz Waves*, Oct. 2011, pp. 1–2.
[39] D. Hasan and C. Lee, "Hybrid metamatarial absorber enhanced sensing of Co_2 gas in the 5–8 μm mid IR spectral window," in *Proc. 19th Int. Conf. Solid-State Sensors, Actuat. Microsyst.*, Jun. 2017, pp. 664–667.
[40] B. Ni, Z. Y. Wang, R. S. Zhao, X. Y. Ma, Z. Q. Xing, L. S. Yang, L. J. Huang, Y. Y. Lin, and D. B. Zhang, "Humidity sensor based on perfect metamaterial absorber," in *Proc. Int. Conf. Numer. Simul. Optoelectron. Devices (NUSOD)*, Jul. 2016, pp. 37–38.
[41] M. Amiri, M. Abolhasan, N. Shariati, and J. Lipman, "RF-Self-Powered sensor for fully autonomous soil moisture sensing," *IEEE Trans. Microw. Theory Techn.*, vol. 71, no. 3, pp. 1374–1387, Mar. 2023.
[42] M. Amiri, M. Abolhasan, N. Shariati, and J. Lipman, "Remote water salinity sensor using metamaterial perfect absorber," *IEEE Trans. Antennas Propag.*, vol. 70, no. 8, pp. 6785–6794, Aug. 2022.
[43] H. K. Kim, M. Yoo, and S. Lim, "Novel ethanol chemical sensor using microfluidic metamaterial," in *Proc. IEEE Int. Symp. Antennas Propag. USNC/URSI Nat. Radio Sci. Meeting*, Jul. 2015, pp. 1358–1359.
[44] B.-X. Wang, G.-Z. Wang, T. Sang, and L.-L. Wang, "Six-band terahertz metamaterial absorber based on the combination of multiple-order responses of metallic patches in a dual-layer stacked resonance structure," *Sci. Rep.*, vol. 7, no. 1, p. 41373, Jan. 2017.
[45] K. V. Sreekanth, M. ElKabbash, Y. Alapan, A. R. Rashed, U. A. Gurkan, and G. Strangi, "A multiband perfect absorber based on hyperbolic metamaterials," *Sci. Rep.*, vol. 6, no. 1, p. 26272, May 2016.
[46] C. Gong, M. Zhan, J. Yang, Z. Wang, H. Liu, Y. Zhao, and W. Liu, "Broadband terahertz metamaterial absorber based on sectional asymmetric structures," *Sci. Rep.*, vol. 6, no. 1, p. 32466, Aug. 2016.
[47] H. Huang, H. Xia, W. Xie, Z. Guo, H. Li, and D. Xie, "Design of broadband graphene-metamaterial absorbers for permittivity sensing at mid-infrared regions," *Sci. Rep.*, vol. 8, no. 1, p. 4183, Mar. 2018.
[48] S. B. Heymsfield, Z. Wang, R. N. Baumgartner, and R. Ross, "Human body composition: Advances in models and methods," *Annu. Rev. Nutrition*, vol. 17, no. 1, pp. 527–558, Jul. 1997.
[49] M. Kara, "Effects of substrate thickness on the properties of rectangular microstrip antenna elements," in *Proc. AMPC Asia–Pacific Microw. Conf.*, vol. 1, 1992, pp. 203–206.
[50] M. Aalizadeh, A. Khavasi, B. Butun, and E. Ozbay, "Large-area, cost-effective, ultra-broadband perfect absorber utilizing manganese in metal-insulator-metal structure," *Sci. Rep.*, vol. 8, no. 1, p. 9162, Jun. 2018.
[51] I. D. Flintoft, M. P. Robinson, G. C. R. Melia, A. C. Marvin, and J. F. Dawson, "Average absorption cross-section of the human body measured at 1–12 GHz in a reverberant chamber: Results of a human volunteer study," *Phys. Med. Biol.*, vol. 59, no. 13, pp. 3297–3317, Jul. 2014.
[52] K. Harima, "Estimation of power absorbed by human body using reverberation chamber," in *Proc. IEEE Int. Symp. Electromagn. Compat.*, Aug. 2012, pp. 39–43.
[53] A. Hirata, I. Laakso, T. Oizumi, R. Hanatani, K. H. Chan, and J. Wiart, "The relationship between specific absorption rate and temperature elevation in anatomically based human body models for plane wave exposure from 30 MHz to 6 GHz," *Phys. Med. Biol.*, vol. 58, no. 4, pp. 903–921, Feb. 2013. [Online]. Available: http://stacks.iop.org/0031-9155/58/i=4/a=903

FARZAD TOFIGH (Member, IEEE) received the Ph.D. degree from the University of Technology Sydney (UTS), in 2019, focusing on non-intrusive techniques for estimating crowd density through the use of distributed sensor networks (IoT) and an innovative approach that utilizes electromagnetic energy monitoring. At UTS, he was involved in various research initiatives, developing and deploying IoT solutions for the university's industry partners. He is currently a Research Fellow at the Cyber Digital Centre (CDC) at UTS. His research interests include wireless sensing and communication, intelligent signal processing, and distributed estimation techniques.

JUSTIN LIPMAN (Senior Member, IEEE) fosters innovation in connected technologies and thrives at the intersection of academia and industry. As an Industry Associate Professor and Director of the Cyber Digital Centre (CDC) at the University of Technology Sydney, he leverages over 12 years of Research and Development expertise at Intel and Alcatel. Previously at UTS, he was Director of the RF and Communications Technologies Laboratory and served as Deputy Chief Scientist of the Food Agility Cooperative Research Centre. He has secured over $35M in research funding, driving innovation across cybersecurity, RF, the IoT, digital agriculture, smart cities, and data privacy. He actively shapes future connected systems through standards development. As a dedicated bridge builder, he fuels impactful industry collaborations translating research into real-world solutions. He holds 24 U.S. patents and has published over 130 peer-reviewed articles.